[6] E. Candes, "The restricted isometry property and its implications for compressed sensing," *Compte Rendus de l'Academie des Sciences, Paris, Serie I*, vol. 346, no. 9/10, pp. 589–592, May 2008.
[7] E. Candes, J. Romberg, and T. Tao, "Robust uncertainty principles: Exact signal reconstruction from highly incomplete frequency information," *IEEE Trans. Inf. Theory*, vol. 52, no. 2, pp. 489–509, Feb. 2006.
[8] E. Candes and T. Tao, "Near-optimal signal recovery from random projections: Universal encoding strategies," *IEEE Trans. Inf. Theory*, vol. 52, no. 12, pp. 5406–5425, Dec. 2006.
[9] R. Chan, C.-W. Ho, and M. Nikolova, "Salt-and-pepper noise removal by median-type noise detectors and detail-preserving regularization," *IEEE Trans. Image Process.*, vol. 14, no. 10, pp. 1479–1485, Oct. 2005.
[10] P. Civicioglu, "Using uncorrupted neighborhoods of the pixels for impulsive noise suppression with ANFIS," *IEEE Trans. Image Process.*, vol. 16, no. 3, pp. 759–773, Mar. 2007.
[11] W. Dai and O. Milenkovic, "Subspace pursuit for compressive sensing signal reconstruction," *IEEE Trans. Inform. Theory*, vol. 55, no. 5, pp. 2230–2249, May 2009.
[12] D. Donoho, "Compressed sensing," *IEEE Trans. Inf. Theory*, vol. 52, no. 4, pp. 1289–1306, Apr. 2006.
[13] D. Donoho, Y. Tsaig, I. Drori, and J. Starck, Sparse solution of underdetermined linear equations by stagewise orthogonalmatching pursuit 2006, Preprint.
[14] M. Figueiredo, R. Nowak, and S. Wright, "Gradient projection for sparse reconstruction: Application to compressed sensing and other inverse problems," *IEEE J. Sel. Topics Signal Process.*, vol. 1, no. 4, pp. 586–597, Dec. 2007.
[15] R. Garg and R. Khandekar, "Gradient descent with sparsification: An iterative algorithm for sparse recovery with restricted isometry property," in *Proc. ICML*, 2009, pp. 337–344.
[16] E. Hale, W. Yin, and Y. Zhang, A fixed-point continuation method for ℓ_1 regularized minimization with applications to compressed sensing Rice University (CAAM), Houston, TX, Tech. Rep. TR07-07, 2007.
[17] T. Hashimoto, "Bounds on a probability for the heavy tailed distribution and the probability of deficient decoding in seequential decoding," *IEEE Trans. Inf. Theory*, vol. 51, no. 3, pp. 990–1002, Mar. 2005.
[18] J. Haupt and R. Nowak, "Compressive sampling vs. conventional imaging," in *Proc. ICIP*, 2006, pp. 1269–1272.
[19] J. Haupt and R. Nowak, "Signal reconstruction from noisy random projections," *IEEE Trans. Inf. Theory*, vol. 52, no. 9, pp. 4036–4048, 2006.
[20] P. J. Huber, *Robust Statistics*. New York: Wiley, 1981.
[21] D. Hunter and K. Lange, "A tutorial on MM algorithms," *Amer. Stat.*, vol. 58, no. 1, pp. 30–37, 2004.
[22] S. Ji, Y. Xue, and L. Carin, "Bayesian compressive sensing," *IEEE Trans. Signal Process.*, vol. 56, no. 6, pp. 2346–2356, Jun. 2008.
[23] S.-J. Kim, K. Koh, M. Lustig, S. Boyd, and D. Gorinevsky, "A method for large-scale ℓ_1-regularized least squares," *IEEE J. Sel. Topics Signal Process.*, vol. 4, no. 1, pp. 606–617, 2007.
[24] K. Koh, S.-J. Kim, and S. Boyd, "An interior-point method for large-scale l_1-regularized logistic regression," *J. Mach. Learn. Res.*, vol. 8, pp. 1519–1555, Dec. 2007.
[25] M. Lustig, D. Donoho, and J. M. Pauly, "Sparse MRI: The application of compressed sensing for rapid MR imaging," *Magn. Reson. Med.*, vol. 58, no. 6, pp. 1182–1195, Dec. 2007.
[26] S. G. Mallat and Z. Zhang, "Matching pursuit with time-frequency dictionaries," *IEEE Trans. Signal Process.*, vol. 41, no. 12, pp. 3397–3415, Dec. 1993.
[27] D. Middleton, "Non-Gaussian noise models in signal processing for telecommunications:new methods and results for class A and class B noise models," *IEEE Trans. Inf. Theory*, vol. 45, no. 4, pp. 1129–1149, May 1999.
[28] D. Needell and J. Tropp, "CoSaMP: Iterative signal recovery from incomplete and inaccurate samples," *Appl. Comput. Harmon. Anal.*, vol. 26, no. 3, pp. 301–321, 2009.
[29] Y. Nesterov, Gradient methods for minimizing composite objective function Catholic Univ. Louvain, Leuven, Belgium, Tech. Rep., 2007.
[30] C. L. Nikias and M. Shao, *Signal Processing With Alpha-Stable Distributions and Applications*. Hoboken, NJ: Wiley, 1995.
[31] Y. Tsaig and D. Donoho, "Extensions of compressed sensing," *Signal Process.*, vol. 86, no. 3, pp. 549–571, 2006.
[32] X. Wang and H. V. Poor, "Robust multiuser detection in non-Gaussian channels," *IEEE Trans. Signal Process.*, vol. 47, no. 2, pp. 289–305, Feb. 1999.
[33] P. Windyga, "Fast impulsive noise removal," *IEEE Trans. Image Process.*, vol. 10, no. 1, pp. 173–179, Jan. 2001.

Capacity Analysis For Orthogonal Halftone Orientation Modulation Channels

Orhan Bulan, *Student Member, IEEE*, Vishal Monga, *Member, IEEE*, and Gaurav Sharma, *Senior Member, IEEE*

***Abstract*—Halftone dot orientation modulation has recently been proposed as a method for data hiding in printed images. Extraction of data embedded with halftone orientation modulation is accomplished by computing, from the scanned hardcopy image, detection statistics that uniquely identify the embedded orientation. From a communications perspective, this data hiding setup forms an interesting class of channels with dot orientation as input and a vector of statistics as the output. This paper derives capacity expressions for these channels that allow for numerical evaluation of the capacity. Results provide significant insight for orientation modulation based print-scan resilient data hiding: the capacity varies significantly as a function of the image graylevel and experimentally observed error free data rates closely mirror the variation in capacity.**

***Index Terms*—Capacity, halftone, hardcopy data embedding, orientation modulation channel.**

I. Introduction

Hardcopy data embedding, i.e., data embedding in images that are intended to survive the print-scan process, continues to be an area of significant interest. Applications lie in document authentication, tamper prevention and detection, tracking/inventory control, and meta-data embedding. While hardcopy data embedding shares several generic concerns with robust watermarking, the major distinguishing factor is the presence of the print-scan distortion channel.

Continuous grayscale images are typically binarized or halftoned before printing. A large number of binary representations provide a perceptually acceptable representation of a given continuous image. The flexibility available in choosing among these binary patterns provides an avenue for data embedding. A significant class of methods [2]–[5] utilize oriented binary patterns for the purpose of embedding, including our recent proposal [5] upon which we base our subsequent discussion. Our method adapts classical clustered dot halftoning [6], which is used widely in laser printers, for hiding data in hardcopy images via halftone dot orientation modulation. Our modifications of the halftoning process

Manuscript received October 20, 2010; revised March 07, 2011 and April 25, 2011; accepted May 02, 2011. Date of publication May 19, 2011; date of current version December 16, 2011. This work was supported in part by a grant from Xerox Corporation and by a grant from New York State Office of Science, Technology & Academic Research (NYSTAR) through the Center for Emerging and Innovative Sciences (CEIS). An earlier version of this paper was presented at the IEEE ICASSP, Las Vegas, NV, April 2008. The associate editor coordinating the review of this manuscript and approving it for publication was Dr. Stefan Winkler.

O. Bulan is with the Department of Electrical and Computer Engineering, University of Rochester, Rochester, NY 14627-0126 USA (e-mail: bulan@ece.rochester.edu).

V. Monga is with the Department of Electrical Engineering, Pennsylvania State University, University Park, PA 16802 USA. Part of this work was conducted while he was with Xerox Research Center, Webster, NY 14580 USA (e-mail: vmonga@engr.psu.edu).

G. Sharma is with the Department of Electrical and Computer Engineering, the Department of Biostatistics and Computational Biology, and the Department of Oncology, University of Rochester, Rochester, NY 14627-0126 USA (e-mail: gaurav.sharma@rochester.edu).

Color versions of one or more of the figures in this paper are available online at http://ieeexplore.ieee.org.

Digital Object Identifier 10.1109/TIP.2011.2155078

imply that for a constant gray area the binary halftone dot is elliptically (as opposed to circularly) shaped.[1] When combined with a coordinate transform, this permits dot-orientation control and hence data embedding proceeds by a choice of orientation (or by quantization in orientation). Dot orientation based embedding is attractive for two major reasons. First, orientation exhibits robustness under printing and scanning because variations in the printer and scanner graylevel "tone" responses do not directly impact dot orientation. Second, a change of orientation alone does not change the area covered by the dot. Thus average graylevel of local regions is preserved under orientation modulation, a trait that is advantageous in cases where maintaining faithfulness to printed image quality is important.

Data extraction is accomplished by identifying the embedded orientation for each of the elliptical halftone dots from a scan of the printed image. This typically involves the computation of suitable detection statistics corresponding to each of the dots, based on which the embedding orientation is estimated. Alternatively, if error correction coding is employed, the detection statistics for the image are collectively utilized for decoding the embedded data. Thus data communication takes place over a composite effective channel formed by the combination of the halftoning (with data embedding), printing, scanning, and statistics extraction stages. We refer to this channel as the *orientation modulation channel*. Characterization of this orientation modulation channel is necessary: both in order to adapt the embedding to the characteristics of the channel and to quantify the fundamental limits so that an appropriate error correction code with a suitable code rate can be chosen. A model for the orientation modulation channel was proposed in [5] and preliminary results in forms of capacity upper bounds were provided in [1]. This paper follows up by establishing fundamental limits of such channels. Specifically, we further the work in [1] by providing exact numerical evaluations of the capacity. Additionally, we introduce the notion of "orientation symmetric channels" which provide an accurate approximation for practical orthogonal halftone orientation modulation embedding schemes. We prove formally that for such channels the equiprobable input distribution is indeed the one that achieves capacity.

We note that our analysis is specific to orientation modulation embedding methods. Print-scan channels have been previously investigated in other settings [7]–[9]. Because our analysis encapsulates, within the orientation modulation channel, the entire process from the point where the input orientation is provided for halftone based embedding to the point where detection statistics are computed, print-scan distortions do not need to be modeled at the image level. Instead, by characterizing the orientation modulation channel experimentally, we automatically comprehend these distortions in our analysis in a manner that closely approximates practical use scenarios.

Evaluation of the capacity for experimentally characterized orientation modulation channels reveals that the capacity varies significantly with graylevel and helps to identify hiding friendly graylevels. We also compare the predicted capacity against experimentally obtained error free operational rates obtained with low density parity check codes (LDPC) and repeat accumulate (RA) codes and demonstrate that practical performance closely follows estimated capacity.

[1]In actual practice, the halftone threshold function is modulated and whether oriented dots are produced or not is also dependent on the image graylevel. We refer the reader to [5] for details that we omit here in order to quickly focus attention on our primary problem of interest.

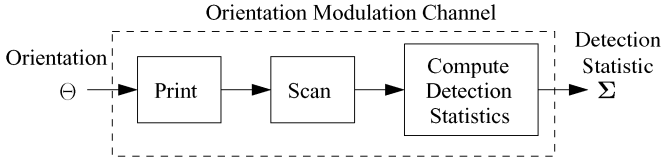

Fig. 1. Orientation modulation channel model.

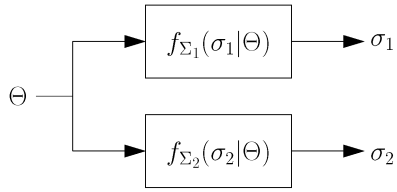

Fig. 2. Simplified probabilistic model for the orientation modulation channel.

The rest of the paper is organized as follows. Section II sets up orientation modulation channels with dot orientation as the input and a detection statistics vector as the output. In Section III, capacity expressions are derived for this class of channels. We introduce and focus our attention specifically on the class of "orientation symmetric channels" that accurately approximate practical orthogonal halftone orientation modulation channels, and simplify analysis by allowing for exact quantification of capacity. In Section IV, we demonstrate an application of the analysis by evaluating and plotting the channel capacity for experimentally characterized clustered-dot halftone data hiding channels utilized in [5]. Section V summarizes concluding remarks.

II. Orientation Modulation Channels

The orientation modulation channel we consider is shown in Fig. 1. In this model, as indicated in the introduction, the channel input is the orientation Θ of the halftone dot and the output is a vector of detection statistics $\mathbf{\Sigma}$ obtained from the printed and scanned version of the dot. These statistics may correspond, for instance, to binary correlations [10], or to image moments estimated from the scans [5]. The detection statistics are computed after synchronization, which we implicitly assume for the modeling and analysis in the present paper.[2] Furthermore, the coverage area for the halftone dots is constrained by the desired graylevel, the capacity of the channel is hence analyzed on a per-graylevel basis.

In practical printing systems, the process of printing inherently introduces a directional asymmetry, which when coupled with arbitrary orientation modulation may result in an unintended and undesirable variation in the average graylevel of the printed halftone. Thus in order to limit perceptible distortion, practical data embedding systems based on orientation modulation often limit the orientations of the dots to two orthogonally oriented directions with respect to which the printing process is symmetric, for example $\pm 45^\circ$ with respect to the direction of paper feed. This symmetry ensures that the orientation modulation causes no change in average graylevel of the printed halftone—thus eliminating (or at least very significantly reducing) potential embedding artifacts. Accordingly for the purpose of estimating capacity, we assume that the input Θ is drawn from a binary alphabet.

For the proposed modeling of the halftone channel, the expression for capacity can be written as [11]

$$C = \max_{p(\theta)} I(\Theta; \mathbf{\Sigma}) = \max_{p(\theta)} \left[h(\mathbf{\Sigma}) - h(\mathbf{\Sigma}|\Theta) \right] \tag{1}$$

[2]A technique for global and local synchronization is described in [5].

where $h(\mathbf{\Sigma})$ denotes the (differential) entropy of the random vector $\mathbf{\Sigma}$ representing the detection statistics, and $h(\mathbf{\Sigma}|\Theta)$ denotes the conditional differential entropy of $\mathbf{\Sigma}$ given the orientation Θ. For binary Θ we can write $h(\mathbf{\Sigma}|\Theta) = \sum_{i=1}^{2} p(\theta_i) h(\mathbf{\Sigma}|\Theta = \theta_i)$ which substituted in the capacity expression of (1), yields

$$C = \max_{p(\theta)} \left[h(\mathbf{\Sigma}) - \sum_{i=1}^{2} p(\theta_i) h(\mathbf{\Sigma}|\Theta = \theta_i) \right]. \tag{2}$$

Although the channel model shown in Fig. 1 is valid for orientation modulation channels with arbitrary detection statistics, in this paper, we specifically focus on moment based detection [5]. In this case, the detection statistics vector $\mathbf{\Sigma}$ comprises of continuous valued moments Σ_1 and Σ_2 evaluated along the two orthogonal directions corresponding to the input modulation [5].

III. Capacity for Orientation Modulation Channels

To quantify fundamental limits, a probabilistic model of the channel in Fig. 1 is required. This is tantamount to modeling the conditional density function $f_{\mathbf{\Sigma}|\Theta}(\sigma_1, \sigma_2|\theta)$. Analytically describing the multi-dimensional density function $f_{\mathbf{\Sigma}|\Theta}(\sigma_1, \sigma_2|\theta)$, however, constitutes a hard task especially, in the absence of a physically inspired model. In order to make the problem tractable, in [5] we assume conditional independence given by

$$f_{\mathbf{\Sigma}|\Theta}(\boldsymbol{\sigma}|\theta) = f_{\Sigma_1|\Theta}(\sigma_1|\theta) f_{\Sigma_2|\Theta}(\sigma_2|\theta) \tag{3}$$

Fig. 2 illustrates the simplified probabilistic model of the orientation modulation channel. In previous work [5], we validated this assumption of conditional independence.[3] (i.e. separability of the probability density function) by estimating the 2×2 covariance matrices (for various graylevels) of the detection statistic vector, and demonstrating that these matrices are substantially diagonal. Under the conditional independence assumption, the joint conditional entropy in (2) is then expressed as $h(\mathbf{\Sigma}|\Theta) = h(\Sigma_1|\Theta) + h(\Sigma_2|\Theta)$. It follows that the capacity becomes

$$C = \max_{p(\theta)} \left[h(\mathbf{\Sigma}) - \sum_{i=1}^{2} p(\theta_i) \left[h(\Sigma_1|\Theta = \theta_i) + h(\Sigma_2|\Theta = \theta_i) \right] \right]. \tag{4}$$

Additionally, the symmetry inherent in the print-scan distortion channel w.r.t orthogonally chosen dot orientations motivates the following symmetry constraints on their conditional densities:

$$f_{\Sigma_1|\Theta}(t|\theta_0) = f_{\Sigma_2|\Theta}(t|\theta_1), \forall t \tag{5}$$

$$f_{\Sigma_1|\Theta}(t|\theta_1) = f_{\Sigma_2|\Theta}(t|\theta_0), \forall t \tag{6}$$

As is shown later in Section IV, the aforementioned conditions in fact accurately approximate experimentally estimated densities. For ease of exposition, from now on we refer to the orientation modulation channels with the symmetry constraints in (5) and (6) as "symmetric orientation channels."

These constraints then imply $[h(\Sigma_1|\theta_1) + h(\Sigma_2|\theta_1)] = [h(\Sigma_1|\theta_0) + h(\Sigma_2|\theta_0)]$. That is, the dependence of the second term in (4) on $p(\theta)$ is eliminated. The capacity is then expressed as

$$\begin{aligned} C &= \max_{p(\theta)} h(\mathbf{\Sigma}) - [h(\Sigma_1|\theta_1) + h(\Sigma_2|\theta_1)] \\ &= \max_{0 \le \alpha \le 1} h_{\mathbf{\Sigma}}(\alpha) - [h(\Sigma_1|\theta_1) + h(\Sigma_2|\theta_1)] \end{aligned} \tag{7}$$

where $\alpha = p(\theta_0)$ and $h_{\mathbf{\Sigma}}(\alpha) = \int f(\mathbf{\Sigma}) \ln f(\mathbf{\Sigma}) d\mathbf{\Sigma}$ with

$$f(\mathbf{\Sigma}) = f(\mathbf{\Sigma}|\theta_0)\alpha + f(\mathbf{\Sigma}|\theta_1)(1-\alpha). \tag{8}$$

[3]Strictly, conditional uncorrelatedness.

The following proposition identifies the capacity achieving distribution in (7).

Proposition 1: For symmetric orientation channels, the equiprobable distribution for $p(\theta)$, i.e., $\alpha = 1/2$, achieves the maxima that defines the capacity.

Proof: The mutual information $I(\Theta; \mathbf{\Sigma})$ is a concave function of the input distribution $p(\theta)$ for a fixed $f_{\mathbf{\Sigma}|\Theta}(\boldsymbol{\sigma}|\theta)$ [11]. For our symmetric orientation channel in (7), this implies that $h(\mathbf{\Sigma})$ is a concave function of $p(\theta)$. We next establish that the equiprobable distribution, i.e. $\alpha = 1/2$ is a stationary point of $h(\mathbf{\Sigma})$ and therefore $I(\Theta; \mathbf{\Sigma})$.

Using conditional independence assumption in (3) and symmetry constraints in (5) and (6), the joint density function of detection statistics can be expanded as

$$\begin{aligned} f_{\mathbf{\Sigma}}(\boldsymbol{\sigma}) = {} & \alpha f_{\Sigma_1|\Theta}(\sigma_1|\theta_0) f_{\Sigma_1|\Theta}(\sigma_2|\theta_1) \\ & + (1-\alpha) f_{\Sigma_1|\Theta}(\sigma_1|\theta_1) f_{\Sigma_1|\Theta}(\sigma_2|\theta_0). \end{aligned} \tag{9}$$

The joint entropy of image moments can then be obtained from (9) as

$$\begin{aligned} h(\mathbf{\Sigma}) = - \int_{-\infty}^{\infty} \int_{-\infty}^{\infty} & [\alpha f(\sigma_1) g(\sigma_2) + (1-\alpha) g(\sigma_1) f(\sigma_2)] \\ & \times \ln [\alpha f(\sigma_1) g(\sigma_2) + (1-\alpha) g(\sigma_1) f(\sigma_2)] \, d\sigma_1 d\sigma_2 \end{aligned} \tag{10}$$

where $f(t) = f_{\Sigma_1|\Theta}(t|\theta_0)$ and $g(t) = f_{\Sigma_1|\Theta}(t|\theta_1)$. The derivative of $h(\mathbf{\Sigma})$ with respect to $p(\theta)$ can be expressed as

$$\begin{aligned} \frac{\partial h(\mathbf{\Sigma})}{\partial \alpha} = - \int_{-\infty}^{\infty} \int_{-\infty}^{\infty} & [f(\sigma_1) g(\sigma_2) - g(\sigma_1) f(\sigma_2)] \\ & \times \ln [\alpha f(\sigma_1) g(\sigma_2) + (1-\alpha) g(\sigma_1) f(\sigma_2)] \, d\sigma_1 d\sigma_2. \end{aligned} \tag{11}$$

By substitution, one can readily verify that $\alpha^* = 1/2$ satisfies the stationary point condition $\partial h(\mathbf{\Sigma})/\partial \alpha = 0$. Thus the equiprobable input distribution is a stationary point of $h(\mathbf{\Sigma})$ and thereby of the mutual information $I(\Theta; \mathbf{\Sigma})$. It follows that equiprobable input distribution achieves the maxima that defines the capacity. In the Appendix, we further show that $h(\mathbf{\Sigma})$ is a strictly concave function of $p(\theta)$ and thus the stationary point $\alpha = 1/2$ corresponds to the unique maximizer. ■

We next consider characterization of conditional densities $f_{\Sigma_1|\Theta}(\sigma_1|\theta)$ and $f_{\Sigma_2|\Theta}(\sigma_2|\theta)$ in order to evaluate the conditional entropy $h(\Sigma_1|\theta_i)$, $h(\Sigma_2|\theta_i)$ in the capacity expression of (7). As in our prior experimental work [5], we use the exponential power density family for modeling the conditional densities. Specifically, we assume that for each $i = 1, 2$, $f_{\Sigma_1|\Theta}(\sigma_1|\theta_i)$ is an exponential power family probability density function with mean μ_{x_i}, scale parameter k_{x_i}, and shape parameter l_{x_i} and $f_{\Sigma_2|\Theta}(\sigma_2|\theta_i)$ is an exponential power family probability density function with mean μ_{y_i}, scale parameter k_{y_i}, and shape parameter l_{y_i}. The channel is then characterized by the parameters $\{\mu_{x_i}, k_{x_i}, l_{x_i}, \mu_{y_i}, k_{y_i}, l_{y_i}\}_{i=1,2}$ and expressions for the conditional densities can be readily obtained from the corresponding expressions for the exponential power density family [12]. For instance,

$$f_{\Sigma_1|\Theta}(\sigma_1|\theta_1) = \frac{l_{x_1}}{2 k_{x_1} \Gamma(1/l_{x_1})} \exp\left(- \left| \frac{\sigma_1 - \mu_{x_1}}{k_{x_1}} \right|^{l_{x_1}} \right). \tag{12}$$

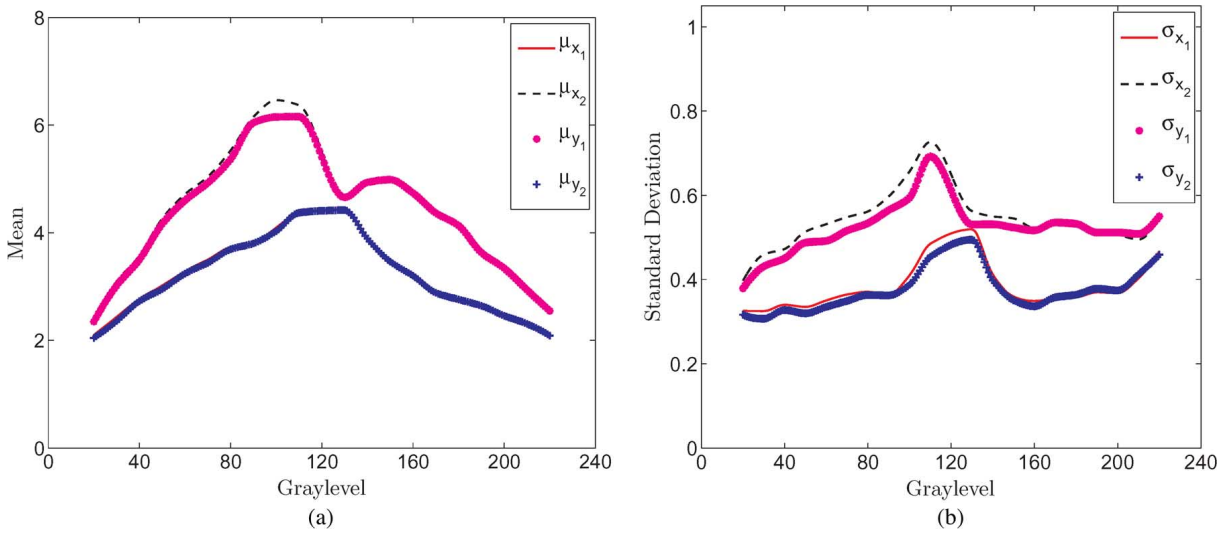

Fig. 3. Experimentally estimated parameters for the conditional density functions. (a) Mean of channel conditional density functions over graylevels. (b) Standard deviation of channel conditional density functions over graylevels.

Substituting the differential entropy of exponential power density family for the conditional entropy terms in (7), the capacity becomes

$$C = h_{\mathbf{\Sigma}}(1/2) - \left[\frac{1}{l_{x_1}} - \ln\left(\frac{l_{x_1}}{2k_{x_1}\Gamma\left(1/l_{x_1}\right)}\right) + \frac{1}{l_{y_1}} - \ln\left(\frac{l_{y_1}}{2k_{y_1}\Gamma\left(1/l_{y_1}\right)}\right)\right]. \quad (13)$$

The capacity can be evaluated by using the above expression with a numerical computation of the $h_{\mathbf{\Sigma}}(1/2)$ term.

The exponential power density family of distributions includes a number of exponential densities commonly used for modeling purposes. In particular, the normal and Laplacian distributions are members of the the exponential power density family. For $l_{x_1} = 1$ the density in (12) corresponds to the Laplacian distribution and for $l_{x_1} = 2$ it becomes the Gaussian distribution with variance $k_{x_1}^2/2$. The situation when all conditional densities are modeled as Gaussians will be of particular interest in our subsequent experimental validation, and we note that in this case, the capacity expression reduces to

$$C = h_{\mathbf{\Sigma}}(1/2) - \left[\ln\left(s_{x_1}\sqrt{2\pi e}\right) + \ln\left(s_{y_1}\sqrt{2\pi e}\right)\right] \quad (14)$$

where the channel conditional densities are $f_{\Sigma_1|\Theta}(\sigma_1|\theta_i) \sim \mathcal{N}(\mu_{x_i}, s_{x_i}^2)$, $f_{\Sigma_2|\Theta}(\sigma_2|\theta_i) \sim \mathcal{N}(\mu_{y_i}, s_{y_i}^2)$, where μ_{x_i} is the mean and s_{x_i} the standard deviation of $f_{\Sigma_1|\Theta}(\sigma_1|\theta_i)$, and other terms are defined similarly. The expression in (14) can also be directly obtained using the well-known [11] expression $\ln(s\sqrt{2\pi e})$ for the differential entropy for a Gaussian random variable with standard deviation s.

IV. Capacity Evaluation for Experimentally Characterized Channels

We demonstrate the variation in capacity with graylevel by using an example experimental set up for which we characterize the channel transition probabilities $f_{\Sigma_1|\Theta}(t|\theta_0)$ and $f_{\Sigma_2|\Theta}(t|\theta_0)$ in (5) and (6) and then utilize these to numerically estimate the channel capacity in (14). Our experimental set up and settings were identical to those in [5]. In order for this description to be largely self-contained we repeat some of the key parameter settings here. Halftone images with clustered elliptical dots with a halftone frequency of 75 lines per inch (lpi) were generated for each graylevel 0, 1, ..., 255 for an 8 bit image representation, where the elliptical dots were oriented along $\pm 45^\circ$ directions depending on the embedded data. The halftone images were then printed on a 2400 dots per inch (dpi) xerographic printer and the resulting printed image is scanned on a flatbed scanner with a 1200 dpi resolution.

To obtain the channel model parameters, we use scans of the printed images corresponding to a graylevel, compute moments along the $\pm 45^\circ$ directions and calculate (conditional) histograms of these moments for each of the orientations. We then determine the channel parameters $\{\mu_{x_i}, k_{x_i}, l_{x_i}, \mu_{y_i}, k_{y_i}, l_{y_i}\}_{i=1,2}$ required for the model of Section III as the values of these parameters for which the modeled conditional densities provide the best least squares fit to the corresponding conditional histograms. We find that the estimated channel conditional densities closely follow the experimentally observed conditional histograms. Also, for most of the graylevels, the shape parameters $\{l_{x_i}, l_{y_i}\}_{i=1,2}$ are found to vary in a narrow interval around 2 indicating that the modeled densities are close to the Gaussian distribution. Based on this observation, for the remainder of the experimental results, we use the Gaussian model for the channel conditional densities, which: a) reduces the parameters to four variables $\{\mu_{x_i}, s_{x_i}\}_{i=1,2}$, allowing easy visualization and b) also enables parameter estimation via expectation maximization [13] during actual decoding, where orientations are unknown *a priori*. Fig. 3 shows the variation of parameters of channel conditional density functions $f_{\Sigma_1|\Theta}(\sigma_1|\theta_0)$, $f_{\Sigma_1|\Theta}(\sigma_1|\theta_1)$, $f_{\Sigma_2|\Theta}(\sigma_2|\theta_0)$, $f_{\Sigma_2|\Theta}(\sigma_2|\theta_1)$ over the graylevels. Correspondingly, Fig. 4(a)–(e) illustrates the channel conditional densities at several graylevels. In Fig. 3, the parameters of $f_{\Sigma_1|\Theta}(\sigma_1|\theta_1)$ and $f_{\Sigma_2|\Theta}(\sigma_2|\theta_0)$, and parameters of $f_{\Sigma_1|\Theta}(\sigma_1|\theta_0)$ and $f_{\Sigma_2|\Theta}(\sigma_2|\theta_1)$ closely follow each other. Similarly, in Fig. 4(a)–(e) corresponding distributions follow each other. Hence, these figures

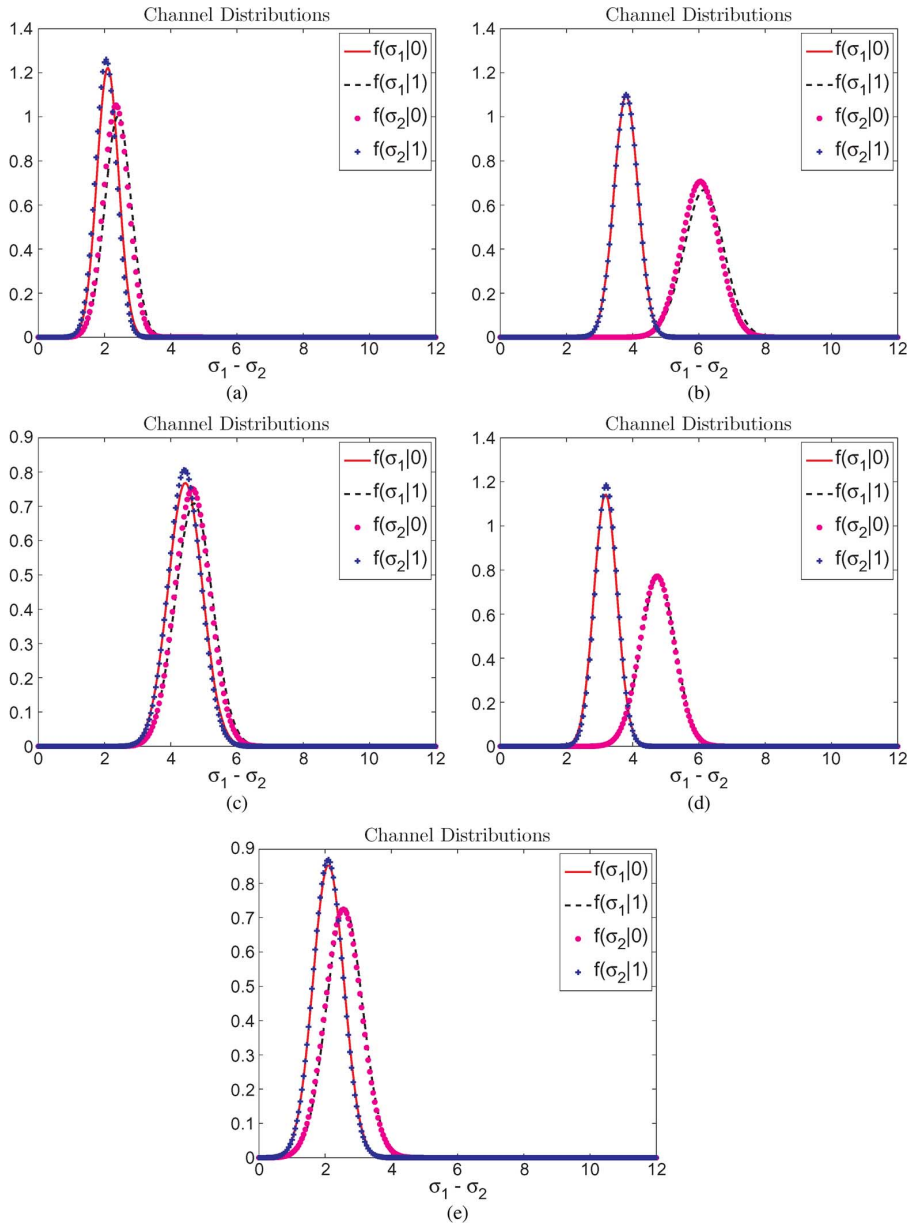

Fig. 4. Estimated conditional probability density functions $\boldsymbol{f}_{\Sigma_1|\Theta}(\boldsymbol{\sigma}_1|\boldsymbol{\theta}_0)$, $\boldsymbol{f}_{\Sigma_1|\Theta}(\boldsymbol{\sigma}_1|\boldsymbol{\theta}_1)$, $\boldsymbol{f}_{\Sigma_2|\Theta}(\boldsymbol{\sigma}_2|\boldsymbol{\theta}_0)$, $\boldsymbol{f}_{\Sigma_2|\Theta}(\boldsymbol{\sigma}_2|\boldsymbol{\theta}_1)$ for the orientation modulation channel at various image graylevels: (a) Graylevel 20; (b) Graylevel 90; (c) Graylevel 130; (d) Graylevel 160; and (e) Graylevel 220.

validate the symmetry constraints on conditional densities in (5) and (6). Furthermore, in Fig. 4(b) and (d) the two groups of distributions are well separated from each other whereas, in Fig. 4(a), (c), and (e) these distributions exhibit substantial overlap. From this observation, it is expected that in graylevels (graylevel 20 (highlight), graylevel 130 (mid-tone), and, graylevel 220 (shadows)) channel capacity must be smaller.

Based on the estimated channel parameters, we then evaluate the capacity expression in (14) over graylevels ranging from white $(\text{digital value} = 0)$ to black $(\text{digital value} = 255)$. For this purpose, we first calculate the joint entropy of detection statistics $h_{\boldsymbol{\Sigma}}(1/2)$ in (14) numerically from experimentally estimated channel parameters for the channel conditional density distributions. A plot of the channel capacity as a function of graylevel is shown in Fig. 6. Below the figure, a ramp function illustrates the halftone-dot orientation modulation at corresponding graylevels in the figure. As is evident from the plot, the capacity is negligibly small in the mid-tones (125–135), highlights (<30) and shadows (>210). The regions between highlights and mid-tones, and between mid-tones and shadows offer significantly higher capacity. The "double hump" shape for the capacity follows intuition as the number of available halftone configurations is severely restricted in highlights, shadows and mid-tones. In the extreme case of purely black or white regions, only a single halftone configuration is possible and hence the capacity is zero. Likewise, the checkerboard configuration of clustered-dot halftones at mid-tones does not provide flexibility for dot orientation. The mismatch in the shape of the two humps is attributed to the asymmetric dot gain that occurs in the physical printing process and is more pronounced in darker as opposed to lighter regions. As noted earlier the print-scan resolutions are automatically accounted for in

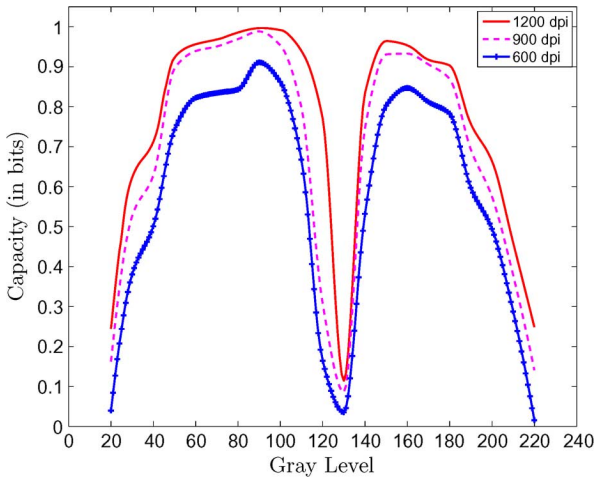

Fig. 5. Capacity for the orientation modulation channel with Gaussian channel conditional distribution as a function of image graylevel at three scan resolutions of 1200 dpi, 900 dpi, and 600 dpi. The graylevel range is from 0 to 255 with 0 corresponding to white and 255 corresponding to black.

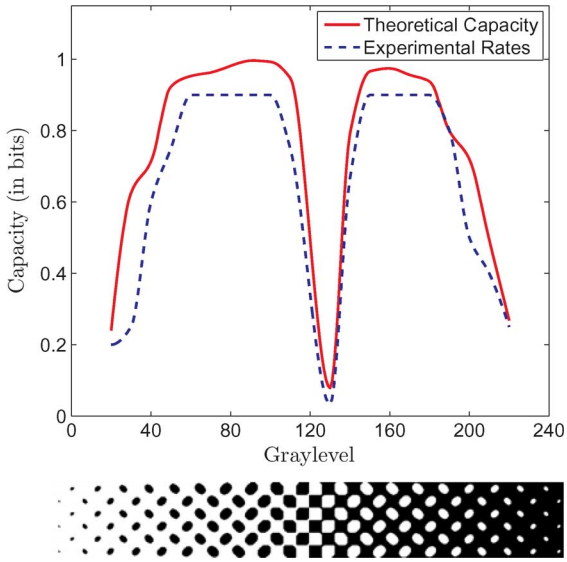

Fig. 6. Capacity for the orientation modulation channel with Gaussian channel conditional distribution as a function of image graylevel. The graylevel range is from 0 to 255 with 0 corresponding to white and 255 corresponding to black. The dashed line on the plot indicates the experimentally attainable error free rate as described in the text.

our analysis framework via the estimation of the channel conditional densities. In order to see the impact of scanner resolution, we also conducted experiments with scan resolutions of 600 and 900 dpi and estimated corresponding channel conditional density functions and evaluated the capacity. The capacity estimates are also included in Fig. 5 (indicated by the legends in the figure). It can be seen that the 600 dpi resolution causes a significant degradation whereas the 900 dpi scan resolution is only slightly worse than the 1200 dpi, which is why the latter was chosen for our experimental setting.

The graph in Fig. 6 compares the capacity (for our 1200 dpi chosen experimental setting) to experimentally determined error free operational rate as a function of graylevel (shown by the dashed line in the plot). These rates are obtained by using LDPC/RA codes along with a simulation of the print-scan process where the channel outputs for a given binary orientation are obtained by randomly sampling a dot of the corresponding orientation from a scan of a print of the target graylevel containing random data embedded via orientation modulation. This closely approximates actual printing and scanning while eliminating the need to tediously print and scan pages carrying error correction coded data for a variety of rates. From the graph, we observe that the experimentally observed achievable error free rates closely follow the capacity. Note that the plateau observed for a rate of 0.9 (in the middle regions of the two humps) corresponds to the maximum rate code utilized in the experiments.

Note that the relative variation of capacity as a function of graylevel in Fig. 6 is tied closely to dot-orientation modulation in clustered-dot halftoning and moment based detection. For other orientation based schemes, the capacity expression as derived in Section III still holds but will require corresponding models and estimation of channel parameters for numerical evaluation of capacity. Also, in this paper, we have focused primarily on the variation in capacity as a function of graylevel and the plots of Figs. 5 and 6 are therefore based on channel parameters estimated from constant graylevel images. In practice, when using orientation modulation for data hiding, texture in the cover image may also cause interference with halftone orientation modulation. The impact of such interference is dependent on the scale of the texture in relation to the halftone frequency and the trade-off invoked between image fidelity and robustness of the data recovery during the joint halftoning and data hiding process; versions prioritizing image quality [5] and robustness of data extraction [14] have both been employed. The exact choice will be application and system dependent and a full investigation of the trade-offs is beyond the scope of this paper. We note, however, that if the scale of the texture is much larger than the halftone frequency, or if one gives priority to robustness of the data encoding over image quality,[4] the achievable rates will closely follow the rates that we present in Fig. 6. If on the other hand, the image textures contain significant energy at the halftone frequency, the interference caused by the textures in the halftone modulation process will usually reduce the achievable rates in comparison to the results shown in Fig. 6.

V. Conclusion

We investigate the capacity of orientation modulation channels manifested in schemes for data hiding in printed halftone images, where control of dot-orientation is exercised for embedding data. Many of these schemes use two orthogonal orientations, which are desirable from the viewpoint of minimizing perceived distortion. We argue that symmetry constraints apply in such cases to channel conditional densities and use these constraints to establish that an equiprobable input distribution achieves capacity for such "symmetric orientation channels". For data hiding via clustered-halftone dot orientation modulation, we estimate channel parameters and numerically evaluate capacity for each graylevel. Results provide crucial insights for orientation-modulation-based print-scan resilient data hiding. In particular, highlights, shadows and mid-tones offer small capacity, whereas high capacity is available in regions from white to mid-tone and mid-tone to black. Experimental achievable error free rates are shown to closely follow the variation in capacity.

[4]When the scale of the textures is smaller than the halftone frequency, the fidelity of texture reproduction is rather limited even if given priority.

APPENDIX

In Section III we showed that the equiprobable distribution, i.e. $\alpha = 1/2$, is a stationary point of $h(\mathbf{\Sigma})$ and therefore $I(\Theta; \mathbf{\Sigma})$. Thus, it achieves the maxima that defines the capacity. Here, we further show that when the capacity is non-zero, $h(\mathbf{\Sigma})$ is a strictly concave function of α and hence the equiprobable distribution is the unique maximizer for the mutual information $I(\Theta; \mathbf{\Sigma})$.

The second derivative of $h(\mathbf{\Sigma})$ can be calculated as:

$$\frac{\partial^2 h(\mathbf{\Sigma})}{\partial^2 \alpha} = \int_{-\infty}^{\infty}\int_{-\infty}^{\infty} -\left[f(\sigma_1)g(\sigma_2) - g(\sigma_1)f(\sigma_2)\right]^2 \times \left[\alpha f(\sigma_1)g(\sigma_2) + (1-\alpha)g(\sigma_1)f(\sigma_2)\right]^{-1} d\sigma_1 d\sigma_2 \tag{15}$$

Note that $(\partial^2 h(\mathbf{\Sigma})/\partial^2 \alpha) \leq 0$ because both $[f(\sigma_1)g(\sigma_2) - g(\sigma_1)f(\sigma_2)]^2$ and $[\alpha f(\sigma_1)g(\sigma_2) + (1-\alpha)g(\sigma_1)f(\sigma_2)]$ are non-negative for all values of $0 \leq \alpha \leq 1$. Further, $(\partial^2 h(\mathbf{\Sigma})/\partial^2 \alpha) = 0$ can hold only if $f(\sigma_1)g(\sigma_2) = g(\sigma_1)f(\sigma_2)$, $\forall \sigma_1, \sigma_2$. This in general entails that $f(t) = cg(t)$ for some constant c. Because $f()$, $g()$ are probability density functions, it follows that $c = 1$. It is easy to see that this rather trivial case of $f(t) = g(t)$ drives the mutual information $I(\Theta; \mathbf{\Sigma})$ and hence the capacity to zero regardless of what α is chosen. Therefore, for all other $f()$, $g()$, we have $(\partial^2 h(\mathbf{\Sigma})/\partial^2 \alpha) < 0$. It then follows that $h(\mathbf{\Sigma})$ is a strictly concave function of α.

ACKNOWLEDGMENT

The authors thank P. Moulin for suggesting that they explore exact numerical evaluation of capacity instead of the bounds previously reported in [1]. The authors also thank anonymous reviewers of their related paper [5], who rekindled their interest in the analysis through their remarks on that manuscript.

REFERENCES

[1] O. Bulan, G. Sharma, and V. Monga, "On the capacity of orientation modulation halftone channels," in *Proc. IEEE Intl. Conf. Acoust. Speech and Signal Process.*, Las Vegas, NV, Apr. 2008, pp. 1685–1688.

[2] C. Liu, S. Wang, and B. Xu, "Authenticate your digital prints with Glossmark images," in *Proc. IS&T NIP20: Int. Conf. on Digital Printing Technologies*, Oct. 2004, pp. 312–316.

[3] D. L. Hecht, "Printed embedded data graphical user interfaces," *IEEE Computer*, vol. 34, no. 3, pp. 47–55, Mar. 2001.

[4] O. Bulan, V. Monga, and G. Sharma, "High capacity color barcodes using dot orientation and color separability," in *Proc. SPIE: Media Forensics and Security XI*, E. J. D. , III, J. Dittmann, N. D. Memon, and P. W. Wong, Eds., Jan. 2009, vol. 7254, p. 725 417-1-7.

[5] O. Bulan, G. Sharma, and V. Monga, "Orientation modulation for data hiding in clustered-dot halftone prints," *IEEE Trans. Image Process.*, vol. 19, no. 8, pp. 2070–2084, Aug. 2010.

[6] R. J. Pellar and L. Green, "Electronic halftone generator," U.S. Patent 4 149 183, Apr. 10, 1979.

[7] S. Voloshynovskiy, O. Koval, R. Villán, E. Topak, J. E. Vila-Forcén, F. Deguillaume, Y. Rytsar, and T. Pun, "Information-theoretic analysis of electronic and printed document authentication," in *Proc. SPIE-IS&T Electron. Imag. 2006, Security, Steganography, and Watermarking of Multimedia Contents VIII*, San Jose, CA, Jan. 15–19, 2006, pp. 15–19.

[8] R. Villán, S. Voloshynovskiy, O. Koval, J. Vila-Forcén, E. Topak, F. Deguillaume, Y. Rytsar, and T. Pun, "Text data-hiding for digital and printed documents: Theoretical and practical considerations," in *Proceedings of SPIE-IS&T Electronic Imaging 2006, Security, Steganography, and Watermarking of Multimedia Contents VIII*, San Jose, USA, January 15–19, 2006, pp. 406–416.

[9] K. Solanki, U. Madhow, B. S. Manjunath, and S. Chandrasekaran, "Modeling the print-scan process for resilient data hiding," in *SPIE Security, Steganography, and Watermarking of Multimedia Contents VII*, Mar. 2005, vol. 5681, pp. 418–429.

[10] D. L. Hecht, "Embedded data glyph technology for hardcopy digital documents," in *Proc. SPIE: Color Hard Copy and Graphic Arts III*, J. Bares, Ed., Mar. 2001, vol. 2171, pp. 341–352.

[11] T. Cover and J. A. Thomas, *Elements of Information Theory*, 2nd ed. Hoboken, NJ: Wiley, 2006.

[12] H. Stark and J. Woods, *Probability, Random Processes, and Estimation Theory for Engineers*, 2nd ed. Englewood Cliffs, NJ: Prentice Hall, 1994.

[13] J. Salojarvi and K. Puolamaki, "Expectation maximization algorithms for conditional likelihoods," in *Proc. 22nd Int. Conf. on Mach. Learn.*, Aug. 2005, pp. 752–759.

[14] O. Bulan, G. Sharma, and B. Oztan, "High capacity image barcodes using color separability," in *Proc. SPIE: Color Imaging XVI: Displaying, Processing, Hardcopy, and Applications*, R. Eschbach, G. G. Marcu, and A. Rizzi, Eds., Jan. , vol. 7866, pp. 20117866-22,1-9.